RADIO SCIENCE, VOL. 48, 1–9, doi:10.1002/rds.20059, 2013

Bridging the gap between the Babinet principle and the physical optics approximation: Vectorial problem

Gildas Kubické,[1] Christophe Bourlier,[2] Morgane Delahaye,[1] Charlotte Corbel,[2] Nicolas Pinel,[2] and Philippe Pouliguen[3]

Received 15 February 2013; revised 29 July 2013; accepted 5 August 2013.

[1] For a three-dimensional problem and by assuming perfectly electric conducting objects, this paper shows that the Babinet principle (BP) can be derived from the physical optics (PO) approximation. Indeed, following the same idea as Ufimtsev, from the PO approximation and in the far-field zone, the field scattered by an object can be split up into a field which mainly contributes around the specular direction (illuminated zone) and a field which mainly contributes around the forward direction (shadowed zone), which is strongly related to the scattered field obtained from the BP. The only difference resides in the integration surface. We show mathematically that the involved integral does not depend on the shape of the object but only on its contour. Simulations are provided to illustrate the link between BP and PO. The main gain of this work is that it provides a more complete physical insight into the connection between PO and BP.

Citation: Kubické, G., C. Bourlier, M. Delahaye, C. Corbel, N. Pinel, and P. Pouliguen (2013), Bridging the gap between the Babinet principle and the physical optics approximation: Vectorial problem, *Radio Sci.*, *48*, doi:10.1002/rds.20059.

1. Introduction

[2] The electromagnetic wave scattering from a target in the forward scattering (FS) region (when the target lies in the transmitter-receiver baseline) [*Siegel*, 1958] is a very interesting phenomenon which was first reported by Mie in 1908 when he discovered that the forward scattered energy produced by a sphere was larger than the backscattered energy [*Glaser*, 1985] in a high-frequency domain. This configuration, which corresponds to a bistatic angle near 180°, is a potential solution to detect stealthy targets. Indeed, in a high-frequency domain and in the forward scattering direction, the RCS (radar cross section) is mainly determined by the silhouette of the target seen by the transmitter and is almost unaffected by absorbing coatings or shapings. This phenomenon can be physically explained by the fact that the scattered field in the forward direction represents the perturbation to the incident wave as a blocking effect, which creates a shadowed zone behind the target. In this region, while the total field vanishes, the scattered field tends to the incident field in amplitude but with opposite phase. A simple explanation can be given using the Babinet principle [*Siegel*, 1958] (BP), which states that the diffraction pattern (in the forward direction) of an opaque body is identical to that of a hole (in a perfectly conducting screen) having the same shape as its silhouette.

[3] Nevertheless, the physical optics (PO) approximation is sometimes used instead of the BP [*Glaser*, 1985, 1989; *Kildal et al.*, 1996] and provides good results around the forward direction. *Ufimtsev* [2007, 1990, 1992, 2008, 2009] studied the shadow radiation and demonstrated that the PO approximation can be split up into two components [*Ufimtsev*, 2007, 2008]: one which mainly contributes in the backward direction and thus corresponds to a reflected component, and the other one which mainly contributes in the forward direction and thus corresponds to a shadowed component. This last component corresponds to the radiation of a blackbody. Ufimtsev demonstrated that it can be reduced to a contour integral on its shadow contour by applying integral equations and boundary conditions on two objects having the same shadow contour, the shadow contour being the frontier between the illuminated surface and the shadowed surface of an object. Nevertheless, since he considered blackbodies, *Ufimtsev* [2009] did not study theoretically the behavior of the reflected component in the shadow zone.

[4] By contrast, *Gordon* [1975] did not consider a surface of arbitrary shape like Ufimtsev did with blackbodies but applied the physical optics for calculating the diffraction through apertures: this corresponds to the use of BP. Then, he showed that the surface integral on the flat area of the aperture can be reduced to a line integral on the contour of the aperture and demonstrated that this line integral can be analytically computed if the aperture is a polygon. In a more recent study [*Kubické et al.*, 2011] for the scalar case (2-D problems) it was demonstrated that the shadowed

[1]CGN1 Division, Direction Générale de l'Armement, Direction Technique, Maîtrise de l'Information Bruz, France.
[2]Institut d'Electronique et des Télécommunications de Rennes, LUNAM Université, Université de Nantes, Nantes, France.
[3]Direction Générale de l'Armement, Direction de la Stratégie, Mission pour la Recherche et l'Innovation Scientifique, Bagneux, France.

Corresponding author: G. Kubické, CGN1 Division, Direction Générale de l'Armement, Direction Technique, Maîtrise de l'Information, BP7, 35998 Rennes Cedex 9, France. (gildas.kubicke@gmail.com)

0048-6604/13/10.1002/rds.20059

component of PO of an arbitrary-shape object is directly related to BP.

[5] The study is generalized to the vectorial case (3-D problems) for an arbitrary perfectly electric conducting object (not only a blackbody: a perfectly electric conducting (PEC) object being a more general case of the blackbody since the reflection is also considered) in order to obtain a more complete physical insight into the connection between PO and BP. First, a demonstration of the shadow contour theorem, which is different from that of Ufimtsev since an arbitrary perfectly conducting object is considered, is provided. Moreover, the link between the BP and the PO approximations is studied for any object (not only a flat surface as Gordon did): the main conclusion is that BP can be seen as a good approximation of PO in the forward direction. Then, the behavior of the reflected component of PO in the shadow zone is theoretically studied. Last, numerical results compare BP and PO in order to illustrate the theoretical investigations made before. The time convention $e^{+i\omega t}$ is omitted throughout the paper.

2. Theoretical Study

2.1. The Physical Optics (PO) Approximation

[6] Assuming a perfectly conducting target, induced currents on the object surface can be estimated by using the PO approximation. For a 3-D (vectorial) problem, the PO currents are given $\forall \boldsymbol{r} \in \Sigma_{\mathrm{PO}}$ by the well-known expressions (by using the Fresnel reflection coefficients for a PEC object):

$$\begin{cases} \boldsymbol{J}(\boldsymbol{r}) = \hat{\boldsymbol{n}}(\boldsymbol{r}) \times [\boldsymbol{H}_i(\boldsymbol{r}) + \boldsymbol{H}_r(\boldsymbol{r})] \\ \qquad = \hat{\boldsymbol{n}}(\boldsymbol{r}) \times [\boldsymbol{H}_i(\boldsymbol{r}) + \boldsymbol{H}_i(\boldsymbol{r})] \\ \qquad = \frac{A}{\eta_0} \left(\boldsymbol{j}_{\mathrm{PO}} + \boldsymbol{j}_{\mathrm{PO}}\right) \\ \boldsymbol{M}(\boldsymbol{r}) = -\hat{\boldsymbol{n}}(\boldsymbol{r}) \times [\boldsymbol{E}_i(\boldsymbol{r}) + \boldsymbol{E}_r(\boldsymbol{r})] \\ \qquad = -\hat{\boldsymbol{n}}(\boldsymbol{r}) \times [\boldsymbol{E}_i(\boldsymbol{r}) - \boldsymbol{E}_i(\boldsymbol{r})] \\ \qquad = A\,(\boldsymbol{m}_{\mathrm{PO}} - \boldsymbol{m}_{\mathrm{PO}}) \end{cases}, \tag{1}$$

where $(\boldsymbol{E}_r, \boldsymbol{H}_r)$ is the reflected field; $A = E_i(\boldsymbol{0}) e^{-ik_0 \hat{\boldsymbol{k}}_i \cdot \boldsymbol{r}}$ gives the amplitude and the phase of the incident field in vacuum; η_0 is the wave impedance; $\boldsymbol{j}_{\mathrm{PO}} = \hat{\boldsymbol{n}}(\boldsymbol{r}) \times \hat{\boldsymbol{h}}_i(\boldsymbol{r})$, $\boldsymbol{m}_{\mathrm{PO}} = \hat{\boldsymbol{n}}(\boldsymbol{r}) \times \hat{\boldsymbol{e}}_i(\boldsymbol{r})$, $\hat{\boldsymbol{h}}_i$, and $\hat{\boldsymbol{e}}_i$ are the polarizations of the electromagnetic incident field; $\hat{\boldsymbol{n}}$ is the unitary normal vector to the surface; $\boldsymbol{r} = (x, y, z(x,y))$ is a position vector on the surface; $\boldsymbol{J}$ and $\boldsymbol{M}$ are the electric and magnetic currents, respectively; and Σ_{PO} is the target illuminated surface (surface of the object visible from the transmitter). It can be noticed that $z = z(x,y)$ is not a bijective function, and care must be taken to correctly describe the function $z(x,y)$ for any target (for example, for the sphere, such a function $z(x,y)$ has two branches describing the upper and lower hemispheres, respectively). Contrary to the Babinet induced currents (see below), PO currents have a physical meaning (of course, $\boldsymbol{M}(\boldsymbol{r})$ equals 0 in equation (1), but it is written such that two components remain, even if they cancel each other). The radiation of these induced currents in far field (the object is in far field from the receiver), assuming that the incident field is a plane wave being unitary on the target, is obtained $\forall \boldsymbol{r}'$ from the Huygens principle [*Bakker and Copson*, 1939]:

$$\boldsymbol{E}_{\boldsymbol{s},\mathrm{PO}}(\boldsymbol{r}') = G_\infty \boldsymbol{I}_+ + G_\infty \boldsymbol{I}_- = \boldsymbol{E}_{\boldsymbol{s},+}(\boldsymbol{r}') + \boldsymbol{E}_{\boldsymbol{s},-}(\boldsymbol{r}'), \tag{2}$$

where $G_\infty = \left(-ik_0 e^{-ik_0 r'}\right)/(4\pi r')$, $\boldsymbol{r}' = x'\hat{\boldsymbol{x}} + y'\hat{\boldsymbol{y}} + z'\hat{\boldsymbol{z}}$ is the observation vector in the space, $r' = \|\boldsymbol{r}'\|$ and

$$\boldsymbol{I}_\pm = \int_{\Sigma_{\mathrm{PO}}} \left[\boldsymbol{j}_{\mathrm{PO}} - \left(\hat{\boldsymbol{k}}_{\boldsymbol{s}} \cdot \boldsymbol{j}_{\mathrm{PO}}\right) \hat{\boldsymbol{k}}_{\boldsymbol{s}} \pm \boldsymbol{m}_{\mathrm{PO}} \times \hat{\boldsymbol{k}}_{\boldsymbol{s}}\right] e^{i\varphi}\, \mathrm{d}s\,, \tag{3}$$

where $\varphi = k_0(\hat{\boldsymbol{k}}_{\boldsymbol{s}} - \hat{\boldsymbol{k}}_{\boldsymbol{i}}) \cdot \boldsymbol{r}$, $\hat{\boldsymbol{k}}_{\boldsymbol{i}}$ and $\hat{\boldsymbol{k}}_{\boldsymbol{s}}$ are the unitary wave vectors giving the incident and observation directions. $\mathrm{d}s = \mathrm{d}x\, \mathrm{d}y \sqrt{1 + \gamma_x^2 + \gamma_y^2}$ is the surface element, where $\gamma_x = \partial z/\partial x$ and $\gamma_y = \partial z/\partial y$.

[7] The decomposition in equation (2) corresponds to the one proposed by *Ufimtsev* [2007, 2008]. Ufimtsev then showed from numerical results obtained with PO that $\boldsymbol{E}_{\boldsymbol{s},+}(\boldsymbol{r}') = G_\infty \boldsymbol{I}_+$ mainly contributes around the specular direction and thus corresponds to a "reflected" PO component. Moreover, $\boldsymbol{E}_{\boldsymbol{s},-}(\boldsymbol{r}') = G_\infty \boldsymbol{I}_-$ mainly contributes around the forward direction and thus corresponds to a "shadowed" PO component (also called here "forward" PO component).

[8] The unitary wave vectors are defined as

$$\hat{\boldsymbol{k}}_{\boldsymbol{i}} = \begin{bmatrix} \sin\theta_i \cos\phi_i \\ \sin\theta_i \sin\phi_i \\ \cos\theta_i \end{bmatrix}, \hat{\boldsymbol{k}}_{\boldsymbol{s}} = \begin{bmatrix} \sin\theta_s \cos\phi_s \\ \sin\theta_s \sin\phi_s \\ \cos\theta_s \end{bmatrix}, \tag{4}$$

where the spherical angles (θ_i, ϕ_i) and (θ_s, ϕ_s) are the incident and observation angles, respectively (see Figure 1 for the "forward scattering alignment" convention). The scattered field can be written from PO in a spherical coordinate system as

$$\begin{bmatrix} E_{s\theta,\mathrm{PO}} \\ E_{s\phi,\mathrm{PO}} \end{bmatrix} = G_\infty \bar{\boldsymbol{S}}_{\mathrm{PO}} \begin{bmatrix} E_{i\theta} \\ E_{i\phi} \end{bmatrix}, \bar{\boldsymbol{S}}_{\mathrm{PO}} = \begin{bmatrix} S_{\theta\theta} & S_{\theta\phi} \\ S_{\phi\theta} & S_{\phi\phi} \end{bmatrix}, \tag{5}$$

where $\bar{\boldsymbol{S}}_{\mathrm{PO}}$ is the diffraction matrix (Sinclair matrix). By projecting equation (3) in a spherical coordinate system and by using equations (4) and (5) and the fact that $\hat{\boldsymbol{h}}_{\boldsymbol{i}} = \hat{\boldsymbol{k}}_{\boldsymbol{i}} \times \hat{\boldsymbol{e}}_{\boldsymbol{i}}$, we show that the Sinclair matrix can be expressed as

$$\bar{\boldsymbol{S}}_{\mathrm{PO}} = \bar{\boldsymbol{S}}_+ + \bar{\boldsymbol{S}}_-, \tag{6}$$

where

$$\bar{\boldsymbol{S}}_\pm = \int_{\Sigma_{\mathrm{PO}}} \left(\gamma_x \bar{\boldsymbol{A}}_{\mathbf{1}\pm} + \gamma_y \bar{\boldsymbol{A}}_{\mathbf{2}\pm} + \bar{\boldsymbol{A}}_{\mathbf{3}\pm}\right) e^{i\varphi(x,y)}\, \mathrm{d}x\, \mathrm{d}y\,, \tag{7}$$

in which $\bar{\boldsymbol{A}}_{\mathbf{1}\pm} = \left(\bar{\boldsymbol{J}}_{\mathbf{1}} \pm \bar{\boldsymbol{M}}_{\mathbf{1}}\right)$, $\bar{\boldsymbol{A}}_{\mathbf{2}\pm} = \left(\bar{\boldsymbol{J}}_{\mathbf{2}} \pm \bar{\boldsymbol{M}}_{\mathbf{2}}\right)$, $\bar{\boldsymbol{A}}_{\mathbf{3}\pm} = \left(\bar{\boldsymbol{J}}_{\mathbf{3}} \pm \bar{\boldsymbol{M}}_{\mathbf{3}}\right)$, $\varphi(x,y) = xb_1 + yb_2 + z(x,y)b_3$ and

$$\bar{\boldsymbol{J}}_1 = \begin{bmatrix} \sin\theta_s \cos\phi_i & \cos\theta_s \sin\phi_s \sin\theta_i - \cos\theta_i \sin\phi_i \sin\theta_s \\ 0 & \sin\theta_i \cos\phi_s \end{bmatrix}, \tag{8}$$

$$\bar{\boldsymbol{J}}_2 = \begin{bmatrix} \sin\theta_s \sin\phi_i & \cos\theta_i \cos\phi_i \sin\theta_s - \cos\theta_s \cos\phi_s \sin\theta_i \\ 0 & \sin\theta_i \sin\phi_s \end{bmatrix}, \tag{9}$$

$$\bar{\boldsymbol{J}}_3 = \begin{bmatrix} -\cos\theta_s \cos(\phi_s - \phi_i) & -\cos\theta_s \cos\theta_i \sin(\phi_s - \phi_i) \\ \sin(\phi_s - \phi_i) & -\cos\theta_i \cos(\phi_s - \phi_i) \end{bmatrix}, \tag{10}$$

$$\bar{\boldsymbol{M}}_n = -\mathrm{adj}\left(\bar{\boldsymbol{J}}_n\right) = \begin{bmatrix} -J_{n,\phi\phi} & J_{n,\phi\theta} \\ J_{n,\theta\phi} & -J_{n,\theta\theta} \end{bmatrix}, \tag{11}$$

where "adj" corresponds to the adjugate matrix, and

$$\begin{cases} b_1 = k_0 (\sin\theta_s \cos\phi_s - \sin\theta_i \cos\phi_i) \\ b_2 = k_0 (\sin\theta_s \sin\phi_s - \sin\theta_i \sin\phi_i) \\ b_3 = k_0 (\cos\theta_s - \cos\theta_i) \end{cases}. \tag{12}$$

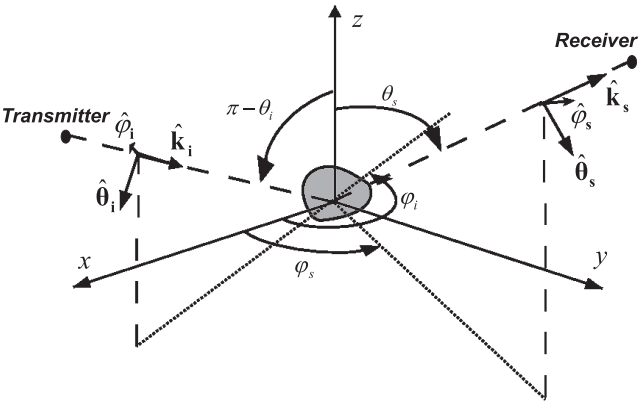

Figure 1. Definition of the convention for wave vectors and angles.

2.2. The Babinet Principle (BP)

[9] The BP is originally an optical principle [*Born and Wolf*, 1959] (generalized to electromagnetics [*Booker*, 1946; *Poincelot*, 1957]) which states that the diffraction pattern of an opaque body is identical to that of a hole having the same shape as its silhouette (see Figure 2). Thus, according to this principle, the FS phenomenon is independent of the shape of the object; the scattering is only due to the target area projected onto the plane orthogonal to the incident direction (see Figure 2): the silhouette of the target. The equivalent induced currents at the aperture are only due to the presence of the incident field:

$$\begin{cases} \boldsymbol{J}(\boldsymbol{r}) = \hat{\boldsymbol{n}}(\boldsymbol{r}) \times \boldsymbol{H}_i(\boldsymbol{r}) = \frac{A}{\eta_0}\boldsymbol{j}_{\mathrm{PO}} \\ \boldsymbol{M}(\boldsymbol{r}) = -\hat{\boldsymbol{n}}(\boldsymbol{r}) \times \boldsymbol{E}_i(\boldsymbol{r}) = -A\boldsymbol{m}_{\mathrm{PO}} \end{cases} \quad \forall \boldsymbol{r} \in \Sigma_{\mathrm{Ba}}. \tag{13}$$

The plane orthogonal to the incident direction splits the space into two subdomains: the backward region Ω_+ and the forward region Ω_- (see Figure 4). Σ_{Ba} is the target area projected onto the plane orthogonal to the incident direction and centered on the phase origin; thus, $\hat{\boldsymbol{n}} = \hat{\boldsymbol{z}}$ in case of normal incidence ($\hat{\boldsymbol{n}}$ being the normal vector to Σ_{Ba} here). It must be noted that the study can be restricted to the normal incidence case without any assumption. Indeed, by rotating the problem, variable changes can be performed to always obtain a local coordinate system in which the incident wave vector direction is in the negative z one. Moving the transmitter with a fixed target is equivalent to rotating the target with a fixed transmitter.

[10] In the far-field zone, the shadow radiation of the BP currents is computed from the Huygens principle, $\forall \boldsymbol{r}' \in \Omega_-$ (Ω_- being the half space behind the object):

$$\boldsymbol{E}_{s,\mathrm{Ba}}(\boldsymbol{r}') = G_\infty \boldsymbol{I}_{\mathrm{Ba}}, \tag{14}$$

with

$$\boldsymbol{I}_{\mathrm{Ba}} = \int_{\Sigma_{\mathrm{Ba}}} \left[\boldsymbol{j}_{\mathrm{PO}} - \left(\hat{\boldsymbol{k}}_s \cdot \boldsymbol{j}_{\mathrm{PO}}\right)\hat{\boldsymbol{k}}_s - \boldsymbol{m}_{\mathrm{PO}} \times \hat{\boldsymbol{k}}_s\right] e^{i\varphi}\, \mathrm{d}s. \tag{15}$$

The shadow radiation can be written from the BP in a spherical coordinate system as

$$\begin{bmatrix} E_{s\theta,\mathrm{Ba}} \\ E_{s\phi,\mathrm{Ba}} \end{bmatrix} = G_\infty \bar{\boldsymbol{S}}_{\mathrm{Ba}} \begin{bmatrix} E_{i\theta} \\ E_{i\phi} \end{bmatrix}, \tag{16}$$

and we show that the Sinclair matrix can be expressed as

$$\bar{\boldsymbol{S}}_{\mathrm{Ba}} = \int_{\Sigma_{\mathrm{Ba}}} \left(\gamma_x \bar{\boldsymbol{A}}_{\mathbf{1}_-} + \gamma_y \bar{\boldsymbol{A}}_{\mathbf{2}_-} + \bar{\boldsymbol{A}}_{\mathbf{3}_-}\right) e^{i\varphi(x,y)}\, \mathrm{d}x\, \mathrm{d}y. \tag{17}$$

Comparing equations (15) and (17) with equations (3) and (7), $\boldsymbol{I}_- = \boldsymbol{I}_{\mathrm{Ba}}$ and $\bar{\boldsymbol{S}}_{\mathrm{Ba}} = \bar{\boldsymbol{S}}_-$ (and thus: $\boldsymbol{E}_{s,-}(\boldsymbol{r}') = \boldsymbol{E}_{s,\mathrm{Ba}}(\boldsymbol{r}')$) if the integral in equation (7) is independent of the shape of the integration surface Σ. This is studied in the next subsection.

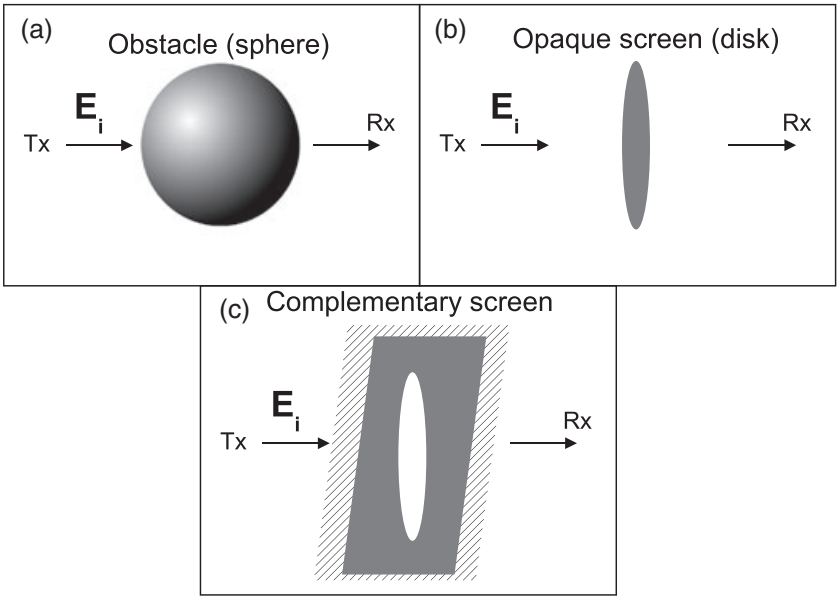

Figure 2. The Babinet principle: (a) forward scattering from an arbitrary obstacle, (b) forward scattering from the associated opaque screen, and (c) diffraction from the complementary screen, that is, a hole in the infinite plane.

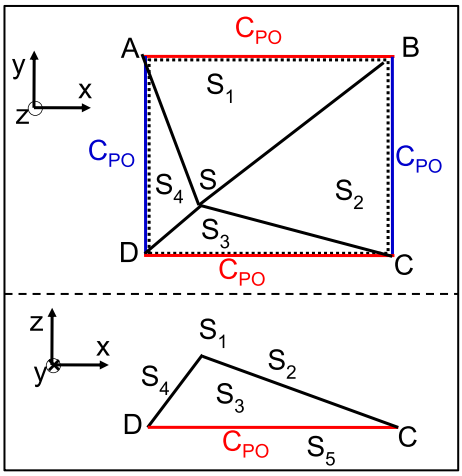

Figure 3. Geometry of the pyramidal target: front view and view from below.

2.3. Proof: "Shadowed" Component

[11] Let C be a positively oriented, piecewise smooth, simple closed curve in a plane, and let Σ be the region bounded by C. By means of Green's theorem, if P and Q are functions of (x, y) defined in an open region containing Σ and have continuous partial derivatives, then

$$\int_{\Sigma}\left(\frac{\partial Q}{\partial x}-\frac{\partial P}{\partial y}\right)\mathrm{d}x\,\mathrm{d}y=\int_{C}(P\,\mathrm{d}x+Q\,\mathrm{d}y), \tag{18}$$

where the path of integration along C is counterclockwise.

[12] Assuming that $b_3 \neq 0$ and since b_1, b_2, and b_3 are independent of x and y:

$$\begin{cases}\frac{\partial\varphi}{\partial x}=b_1+\frac{\partial z}{\partial x}b_3=b_1+\gamma_x b_3\\ \frac{\partial\varphi}{\partial y}=b_2+\frac{\partial z}{\partial y}b_3=b_2+\gamma_y b_3\end{cases}, \tag{19}$$

this implies that

$$\begin{cases}\gamma_x=\frac{1}{b_3}\frac{\partial\varphi}{\partial x}-\frac{b_1}{b_3}\\ \gamma_y=\frac{1}{b_3}\frac{\partial\varphi}{\partial y}-\frac{b_2}{b_3}\end{cases}. \tag{20}$$

[13] Thus, we have

$$\gamma_x\bar{\boldsymbol{A}}_{\mathbf{1}-}+\gamma_y\bar{\boldsymbol{A}}_{\mathbf{2}-}+\bar{\boldsymbol{A}}_{\mathbf{3}-}=\frac{\bar{\boldsymbol{A}}_{\mathbf{1}-}}{b_3}\frac{\partial\varphi}{\partial x}+\frac{\bar{\boldsymbol{A}}_{\mathbf{2}-}}{b_3}\frac{\partial\varphi}{\partial y}+\alpha, \tag{21}$$

where $\alpha = \bar{\boldsymbol{A}}_{\mathbf{3}-} - \bar{\boldsymbol{A}}_{\mathbf{1}-}b_1/b_3 - \bar{\boldsymbol{A}}_{\mathbf{2}-}b_2/b_3$. From equation (17), or from the shadow component $\bar{\boldsymbol{S}}_-$ of equation (7), it is then relevant to set

$$\begin{cases}\frac{\partial P}{\partial y}=\left(-\frac{\alpha}{2}-\frac{\bar{\boldsymbol{A}}_{\mathbf{2}-}}{b_3}\frac{\partial\varphi}{\partial y}\right)e^{i\varphi(x,y)}\\ \frac{\partial Q}{\partial x}=\left(\frac{\alpha}{2}+\frac{\bar{\boldsymbol{A}}_{\mathbf{1}-}}{b_3}\frac{\partial\varphi}{\partial x}\right)e^{i\varphi(x,y)}\end{cases}. \tag{22}$$

Then

$$\begin{cases}P(x,y)=\frac{-\alpha}{2}\int e^{i\varphi(x,y)}\,\mathrm{d}y-\frac{\bar{\boldsymbol{A}}_{\mathbf{2}-}e^{i\varphi(x,y)}}{ib_3}+p(x)\\ Q(x,y)=\frac{\alpha}{2}\int e^{i\varphi(x,y)}\,\mathrm{d}x+\frac{\bar{\boldsymbol{A}}_{\mathbf{1}-}e^{i\varphi(x,y)}}{ib_3}+q(y)\end{cases}, \tag{23}$$

where p and q are any functions of x and y, respectively. From the Green theorem, it is important to note that $\int_C[p(x)\mathrm{d}x+q(y)\mathrm{d}y]=0$, since $\partial p/\partial y=\partial q/\partial x=0$. The substitution of equation (23) into equation (18) and into equation (7) leads to

$$\bar{\boldsymbol{S}}_{\mathrm{PO}}=\bar{\boldsymbol{S}}_{+}+\bar{\boldsymbol{S}}_{-}=\sum_{n=1}^{3}\left(\bar{\boldsymbol{S}}_{n,+}+\bar{\boldsymbol{S}}_{n,-}\right)I_{n,\mathrm{PO}}, \tag{24}$$

where

$$\begin{cases}I_{1,\mathrm{PO}}=-\frac{1}{ib_1}\int_{C_{\mathrm{PO}}}e^{i\varphi(x,y)}\,\mathrm{d}y\\ I_{2,\mathrm{PO}}=\frac{1}{ib_2}\int_{C_{\mathrm{PO}}}e^{i\varphi(x,y)}\,\mathrm{d}x\\ I_{3,\mathrm{PO}}=\iint_{\Sigma_{\mathrm{PO}}}e^{i\varphi(x,y)}\,\mathrm{d}x\,\mathrm{d}y\end{cases}, \tag{25}$$

and

$$\begin{cases}\bar{\boldsymbol{S}}_{1,\pm}=-\frac{b_1}{b_3}\left(\bar{\boldsymbol{J}}_{\mathbf{1}}\pm\bar{\boldsymbol{M}}_{\mathbf{1}}\right)\\ \bar{\boldsymbol{S}}_{2,\pm}=-\frac{b_2}{b_3}\left(\bar{\boldsymbol{J}}_{\mathbf{2}}\pm\bar{\boldsymbol{M}}_{\mathbf{2}}\right)\\ \bar{\boldsymbol{S}}_{3,\pm}=\frac{1}{b_3}\sum_{n=1}^{3}\left(\bar{\boldsymbol{J}}_{\boldsymbol{n}}\pm\bar{\boldsymbol{M}}_{\boldsymbol{n}}\right)b_n\varepsilon_n\end{cases}, \tag{26}$$

in which C_{PO} is the contour of Σ_{PO} (oriented in counterclockwise) so that the integrals $I_{1,\mathrm{PO}}$ and $I_{2,\mathrm{PO}}$ follow the contour of Σ_{PO}. In addition, $\varepsilon_3 = 1$ and $\varepsilon_{1,2} = -1$. Equation (24) shows that the Sinclair Matrix calculated with PO brings three integrals into play. The first two integrals are one dimensional since they are expressed from the contour C_{PO}.

[14] For the PO forward component (minus sign component in equation (24)), it can be shown for all $(\theta_i, \phi_i, \theta_s, \phi_s)$ that

$$\bar{\boldsymbol{S}}_{3,-}=\bar{\mathbf{0}}, \tag{27}$$

where $\bar{\mathbf{0}}$ is the null matrix. Equation (27) clearly shows that the PO forward component is independent of the object

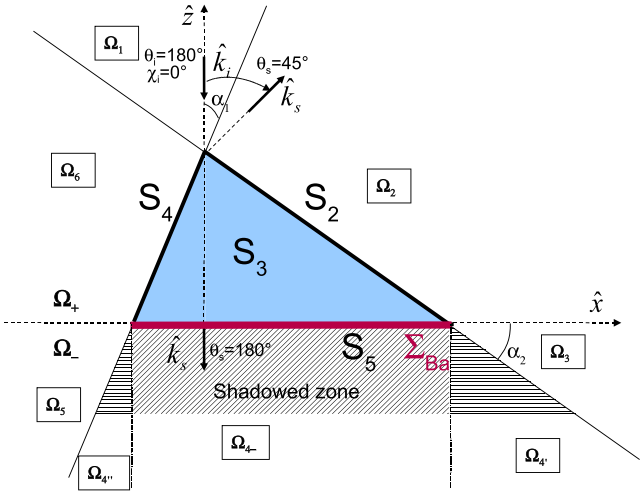

Figure 4. Forward scattering from the pyramidal target of Figure 3, in the view from below (xOz plane). The two associated subdomains Ω_+ ($z > 0$) and Ω_- ($z < 0$) can be split up into $\Omega_+ = \Omega_1 \cup \Omega_2 \cup \Omega_6$ and $\Omega_- = \Omega_3 \cup \Omega_4 \cup \Omega_5$; Ω_4 being defined by an extended shadow zone $\Omega_4 = \Omega_{4'} \cup \Omega_{4-} \cup \Omega_{4''}$. Here $\alpha_1 = \mathrm{atan}(3\lambda/3\lambda) = 45°$ and $\alpha_2 = \mathrm{atan}(3\lambda/7\lambda) \simeq 23.2°$.

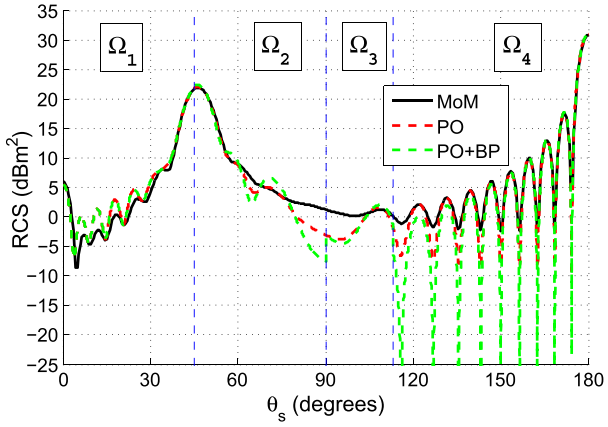

Figure 5. RCS of the pyramidal target for $\theta_i = 180°$ and for VV polarization, computed from the MOM, the PO, and the PO combined with the BP.

shape and depends only on the contour of the illuminated surface (contour C_{PO} in equation (25)) of the object. This is consistent with the "Shadow Contour Theorem" [*Ufimtsev*, 2007, 2008] which states that "The shadow radiation does not depend on the whole shape of the scattering object, and is completely determined only by the size and the geometry of the shadow contour." We emphasize that this was demonstrated with an arbitrary perfectly conducting object, which differs from the works of Ufimtsev and Gordon, as they considered two arbitrary blackbodies (a PEC object being a more general case of the blackbody since the reflection is also considered) and a flat surface, respectively.

[15] From equation (27), the substitution of equation (23) into equation (18) and into equation (17) leads to

$$\bar{\boldsymbol{S}}_{Ba} = \bar{\boldsymbol{S}}_{1,-} I_{1,Ba} + \bar{\boldsymbol{S}}_{2,-} I_{2,Ba}, \tag{28}$$

where

$$\begin{cases} I_{1,Ba} = -\frac{1}{ib_1} \int_{C_{Ba}} e^{i\varphi(x,y)}\, dy \\ I_{2,Ba} = \frac{1}{ib_2} \int_{C_{Ba}} e^{i\varphi(x,y)}\, dx \end{cases}, \tag{29}$$

in which C_{Ba} is the contour of Σ_{Ba} (oriented in counterclockwise). The integrals $I_{1,Ba}$ and $I_{2,Ba}$ follow the contour of Σ_{Ba}.

[16] Thus, from equations (25) and (29), equality between the PO forward component and BP holds if $I_{1,Ba} = I_{1,PO}$ and $I_{2,Ba} = I_{2,PO}$. This is obtained for either

[17] 1. $C_{Ba} = C_{PO}$: the contour of the surface Σ_{PO} is identical to the contour of the surface Σ_{Ba};

or

[18] 2. $\varphi(x,y) = 0$ implying $b_1 = b_2 = b_3 = 0$, which occurs for $\theta_s = \theta_i$ and $\phi_s = \phi_i$: this corresponds to the FS direction, for which $\boldsymbol{k}_i$ and $\boldsymbol{k}_s$ are collinear.

2.4. "Reflected" Component

[19] For the reflected PO component (plus sign in equation (24)), we show for all $(\theta_i, \phi_i, \theta_s, \phi_s)$ that

$$\bar{\boldsymbol{S}}_{3,+} = 2 \begin{bmatrix} a & \sin\phi \\ \sin\phi & -a \end{bmatrix}, \tag{30}$$

where

$$a = \frac{\cos\phi\,(\cos\theta_i \cos\theta_s - 1) + \sin\theta_i \sin\theta_s}{\cos\theta_s - \cos\theta_i}, \tag{31}$$

in which $\phi = \phi_s - \phi_i$. Thus, unlike the field "shadowed component," equation (30) shows that the field in the illuminated zone depends on the surface profile a priori, because the surface integral $I_{3,PO}$ contributes.

2.5. Discussion

[20] In the reflected direction defined by $\theta_s = \pi - \theta_i$ and $\phi_s = \phi_i$ (corresponding to the specular direction for a horizontal plate), we show that

$$\bar{\boldsymbol{S}}_{1,\pm} = \bar{\boldsymbol{S}}_{2,\pm} = \bar{\boldsymbol{S}}_{3,-} = \bar{\boldsymbol{0}}, \tag{32}$$

and

$$\bar{\boldsymbol{S}}_{3,+} = 2 \begin{bmatrix} \cos\theta_i & 0 \\ 0 & -\cos\theta_i \end{bmatrix}. \tag{33}$$

Equation (32) clearly shows that the scattering contribution related to the forward component (minus sign) vanishes in the specular direction. It also highlights that the specular scattered field is only due to the reflected PO component, which strongly depends on the object shape related to the integral $I_{3,PO}$, since, from equations (24) and (33), $\bar{\boldsymbol{S}}_{PO} = S_{3,+} I_{3,PO}$.

[21] In the forward direction defined by $\theta_s = \theta_i$ and $\phi_s = \phi_i$, we show that

$$\begin{cases} \bar{\boldsymbol{S}}_{3,\pm} = \bar{\boldsymbol{S}}_{1,+} = \bar{\boldsymbol{S}}_{2,+} = \bar{\boldsymbol{0}} \\ \bar{\boldsymbol{S}}_{1,-} = 2\cos\theta_i \cos^2\phi_i \bar{\boldsymbol{I}} \\ \bar{\boldsymbol{S}}_{2,-} = 2\cos\theta_i \sin^2\phi_i \bar{\boldsymbol{I}} \end{cases}, \tag{34}$$

where $\bar{\boldsymbol{I}}$ is the identity matrix.

[22] Equation (34) shows that the scattering contribution related to the reflected PO component (plus sign) vanishes in the FS direction and that the scattered field is only due to the forward PO component, which only depends on the contour of the object C_{PO}, since from equations (24) and (34), $\bar{\boldsymbol{S}}_{PO} = S_{1,-} I_{1,PO} + S_{2,-} I_{2,PO} = 2\bar{\boldsymbol{I}} \cos\theta_i (I_{1,PO} \cos^2\phi_i + I_{2,PO} \sin^2\phi_i)$.

[23] In conclusion, we can state that the BP is a good approximation of the PO around the FS direction; that is, $\boldsymbol{E}_{s,Ba} = \boldsymbol{E}_{s,PO}$ when $\boldsymbol{E}_{s,+} \to \boldsymbol{0}$ for a bistatic angle around 180°. The BP exactly matches the PO forward component if the contour of Σ_{Ba} is the same as the one of Σ_{PO}. Then, the BP can be seen as a particular case of the PO approach.

3. Numerical Results

3.1. Combining PO and BP for a Pyramidal Target

[24] Let us consider the scene given in Figure 3, in which a square pyramid is illuminated by an incident plane wave.

[25] The Cartesian coordinates of the apex of the pyramid, which links the four elementary planar surfaces S_1, S_2, S_3, and S_4, is $(-2\lambda, -4\lambda, 3\lambda)$, and the length of a side of the square base S_5 is $L = 10\lambda$. The origin is located at the center of the base S_5. Edge and apex diffractions are neglected because the present work focuses on the FS phenomenon.

[26] Two asymptotic approaches can be considered to compute the RCS of this target. The first one consists in applying the PO approximation on each illuminated surface and then computing the radiation of the induced currents from the Huygens principle for all positions of the receiver.

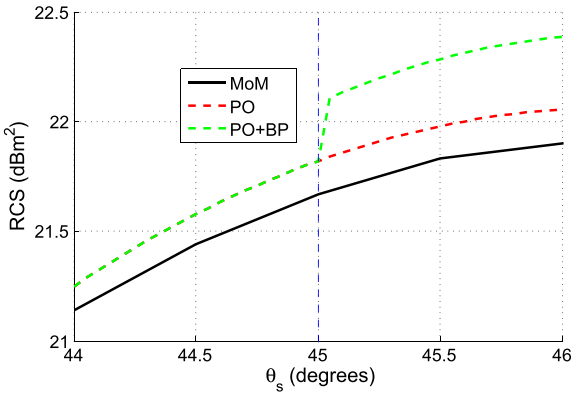

Figure 6. Enlarged detail of Figure 5 around the boundary between Ω_1 and Ω_2.

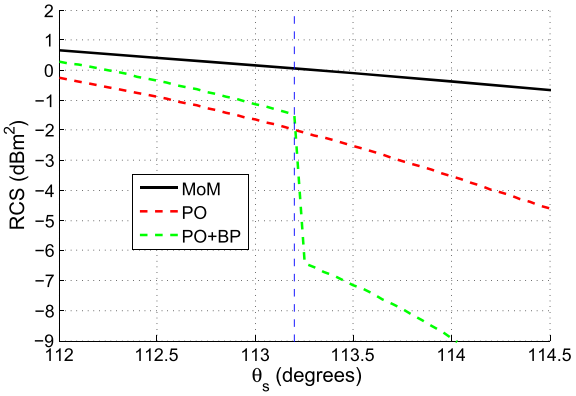

Figure 8. Enlarged detail of Figure 5 around the boundary between Ω_3 and Ω_4.

This takes into account both reflected and forward components of PO for all excited surfaces ($\Sigma_{PO} = S_1 \cup S_2 \cup S_3 \cup S_4$ for a normal incidence for example). The other asymptotic approach combines PO and BP [*Pouliguen et al.*, 2003] (as detailed for the 2-D case in [*Kubické et al.*, 2011]): for a given position of the receiver, PO is applied on surfaces visible from both the transmitter and the receiver (the receiver is in the reflected zone (backward region) of the considered surface) and BP on surfaces which are visible only from the transmitter (the receiver is in an extended shadow zone which correspond to the zone behind the considered surface). Thus, in the extended shadow zone of the whole target, only BP is applied for all four illuminated surfaces. As already discussed for the 2-D case in *Kubické et al.* [2011], combining PO with BP on each elementary surface implies that the reflected PO component is neglected in the extended shadow region of the surfaces where BP is applied. Indeed, it was demonstrated that BP is an approximation of the forward component of PO. Nevertheless, according to PO, the reflected component is much lower than the forward component in the FS direction of a given surface, but this can induce slight discontinuities in the RCS at the subdomains boundaries. Thus, combining PO and BP can be seen as an approximation of PO.

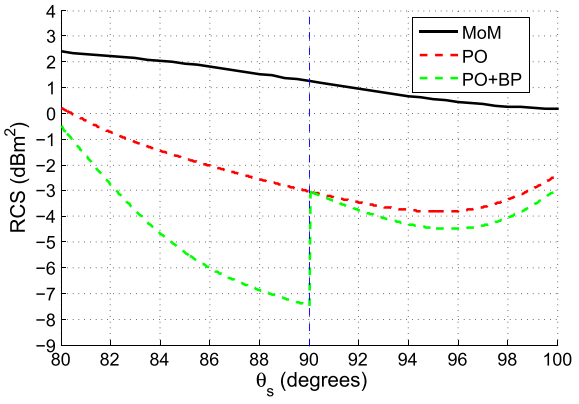

Figure 7. Enlarged detail of Figure 5 around the boundary between Ω_2 and Ω_3.

3.2. First Case: Normal Incidence and VV Polarization

[27] We first consider the normal incidence case, depicted in Figure 4. PO and BP surfaces are $\Sigma_{PO} = S_1 \cup S_2 \cup S_3 \cup S_4$ and $\Sigma_{Ba} = S_5$.

[28] The RCS calculated by these two asymptotic approaches are compared with the RCS computed by a benchmark method: the well-known method of moments (MOM). The comparison is depicted in Figure 5 versus the scattering elevation angle θ_s for $\theta_i = 180°$ (corresponding to an incidence orthogonal to the pyramid base: $\chi_i = 180 - \theta_i = 0°$), $\phi_i = 0°$, and $\phi_s = 0°$ and for VV polarization.

[29] As can be seen, results from the two asymptotic approaches agree well with that of the benchmark method and in particular around the specular direction of surface S_2 ($\theta_s = 45°$) and around the FS direction ($\theta_s = 180°$). Differences between the classical PO and the PO combined with the BP (PO+BP) can be observed for $\theta_s \in [60°; 140°]$. Indeed, the reflected PO component of surface S_4 is set to 0 in Ω_2, the reflected components of surfaces S_1, S_3, and S_4 are set to 0 in Ω_3, and the reflected components of all the surfaces are then set to 0 in $\Omega_4 = \Omega_{4'} \cup \Omega_{4-} \cup \Omega_{4''}$ for the computation of PO+BP, and, as the observation angle increases, these contributions decrease in the classical PO.

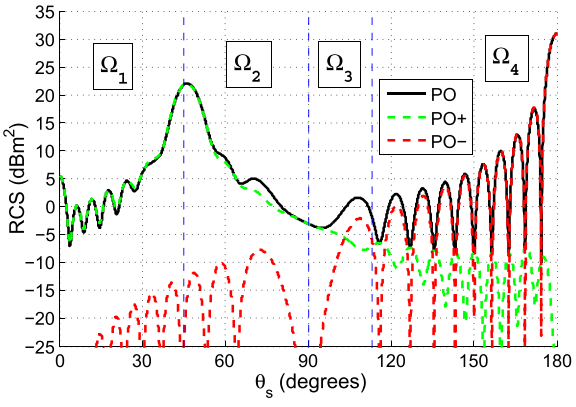

Figure 9. Same simulation parameters as in Figure 5 but computed from PO, PO in reflection, and PO in forward scattering.

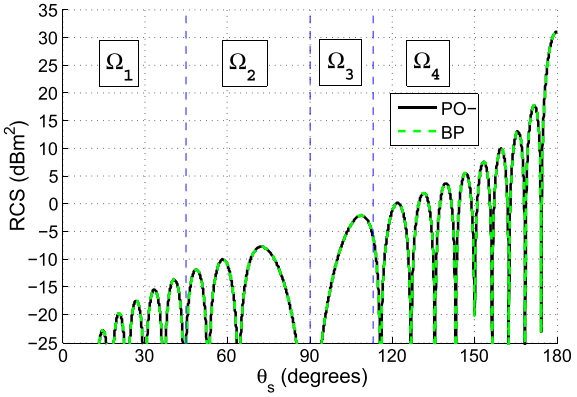

Figure 10. Same simulation parameters as in Figure 5 but computed from PO in forward scattering and BP.

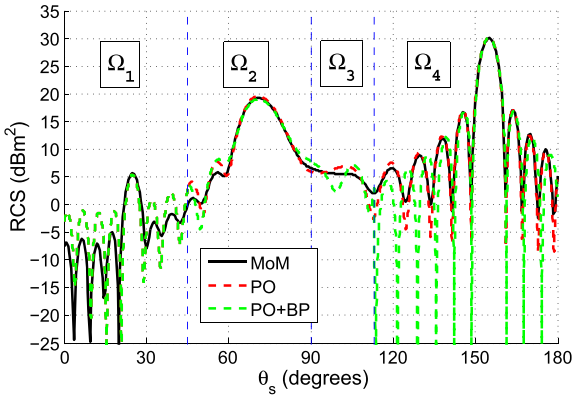

Figure 12. RCS of the pyramidal target for $\theta_i = 155°$ and for VV polarization, computed from the MOM, the PO, and the PO combined with the BP.

Moreover, slight discontinuities in the RCS computed from PO+BP can be observed at the boundaries between the different subdomains Ω_i. The first one occurs at the boundary between Ω_1 and Ω_2 for $\theta_s = \alpha_1 = \text{atan}(3\lambda/3\lambda) = 45°$ (an enlarged detail is depicted in Figure 6). Indeed, from this angle (and higher) the reflected PO component of surface S_1 is set to 0 in PO+BP. The second one occurs at the boundary between Ω_2 and Ω_3 for $\theta_s = 90°$ (an enlarged detail is depicted in Figure 7). Indeed, from this angle (and higher) the reflected PO components of surfaces S_3 and S_4 are set to 0 in PO+BP. The last discontinuity occurs at the boundary between Ω_3 and Ω_4 for $\theta_s = 90° + \alpha_2 = 90° + \text{atan}(3\lambda/7\lambda) = 113.2°$ (an enlarged detail is depicted in Figure 8). Indeed, from this angle (and higher) the reflected PO component of surface S_2 is set to 0 in PO+BP. These discontinuities do not appear with classical PO method (for which the reflected PO components are not set to 0).

[30] Figure 9 compares the RCS computed from the scattered field $\boldsymbol{E}_{s,\text{PO}}$ (PO approach) with the RCS of its two components: the reflected one $\boldsymbol{E}_{s,\text{PO+}}$ and the FS one $\boldsymbol{E}_{s,\text{PO−}}$.

[31] As can be seen, the scattered field from PO is mainly due to the reflected component $\boldsymbol{E}_{s,\text{PO+}}(\boldsymbol{r}')\ \forall \boldsymbol{r}' \in \Omega_1 \cup \Omega_2$. In other words, the reflected component $\boldsymbol{E}_{s,\text{PO+}}(\boldsymbol{r}')$ mainly contributes to the scattering process $\forall \boldsymbol{r}' \in \Omega_1 \cup \Omega_2$. For increasing θ_s from 140°, the reflected component decreases strongly and the FS component becomes the main contribution to the scattered field, $\boldsymbol{E}_{s,\text{PO+}}(\boldsymbol{r}')$ being negligible in the extended shadow zone $\Omega_4 = \Omega_{4'} \cup \Omega_{4-} \cup \Omega_{4''}$. It must be noted that this phenomenon begins to occur in subdominant Ω_3, which is in the reflected zone of S_2.

[32] Figure 10 compares the RCS of the FS component of PO with the RCS obtained by applying BP on the whole target.

[33] A perfect agreement is obtained. This illustrates the proof given in section 2.3. Indeed, here $C_{\text{Ba}} = C_{PO}$: the contour of the surface Σ_{PO} (contour of the surface S_5) is identical to that of the complementary Babinet screen Σ_{Ba}. As theoretically demonstrated, in this case, the Babinet principle is included in PO approach since $\boldsymbol{E}_{s,\text{Ba}}(\boldsymbol{r}') = \boldsymbol{E}_{s,\text{PO−}}(\boldsymbol{r}')$. Interestingly, it can be noted that these results perfectly match the results obtained with other Cartesian coordinates of the apex S: even if the target is different, the same FS component is obtained. The shape of the illuminated surface does not

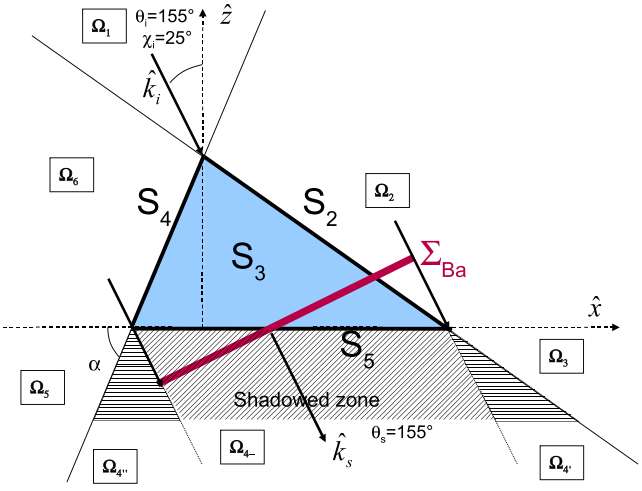

Figure 11. Forward scattering from a pyramidal target with a lateral incidence.

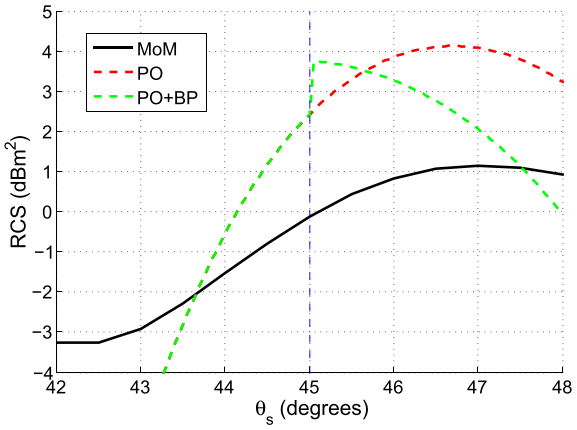

Figure 13. Enlarged detail of Figure 12 around the boundary between Ω_1 and Ω_2.

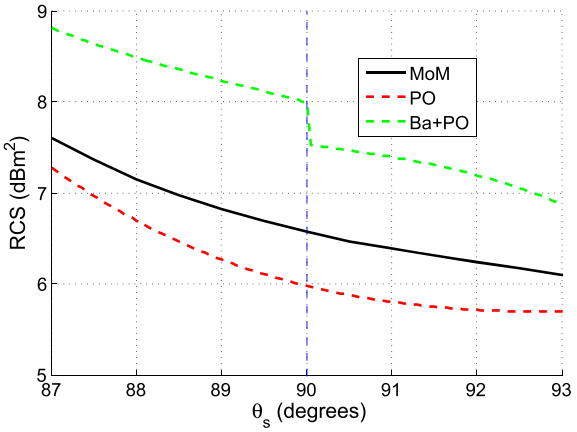

Figure 14. Enlarged detail of Figure 12 around the boundary between Ω_2 and Ω_3.

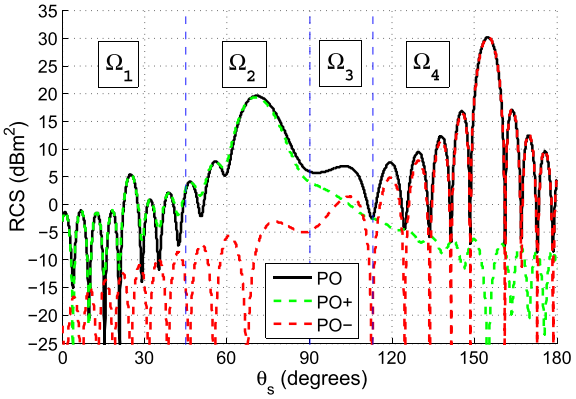

Figure 16. Same simulation parameters as in Figure 12 but computed from PO, PO in reflection, and PO in forward scattering.

play a role, which is consistent with the "Shadow Contour Theorem" [*Ufimtsev*, 2007, 2008].

3.3. Second Case: Lateral Incidence and VV Polarization

[34] We now consider the lateral incidence case, depicted in Figure 11. PO and BP surfaces are $\Sigma_{PO} = S_1 \cup S_2 \cup S_3 \cup S_4$, and Σ_{Ba} corresponds to the projection of the object onto the plane orthogonal to the incident direction (this corresponds to the projection of S_5.)

[35] The RCS of the PO and of the PO combined with the BP approaches are compared with the RCS computed from the MOM in Figure 12 versus the scattering elevation angle θ_s for $\theta_i = 155°$ (corresponding to a lateral incidence: $\chi_i = 180° - \theta_i = 25°$), $\phi_i = 0°$, and $\phi_s = 0°$ and for VV polarization.

[36] Here again, the results from the two asymptotic approaches agree well with that of the benchmark method and in particular around the FS direction ($\theta_s = 180° - \chi_i = 155°$). Some differences between the classical PO and PO+BP can be observed from $\theta_s = 45°$ (and higher). Moreover, three discontinuities in the RCS computed from PO+BP can be observed. The first one occurs at the boundary between Ω_1 and Ω_2 for $\theta_s = 45°$ (an enlarged detail is depicted in Figure 13, in which PO and PO+BP perfectly match for $\theta_s < 45°$ since there is no shadow). The second one occurs at the boundary between Ω_2 and Ω_3 for $\theta_s = 90°$ (an enlarged detail is depicted in Figure 14). The last discontinuity occurs at the boundary between Ω_3 and Ω_4 for $\theta_s = 113.2°$ (an enlarged detail is depicted in Figure 15). Of course, these discontinuities, which are due to the same reasons as detailed before in the first case, do not appear with the classical PO method.

[37] Figure 16 compares the RCS computed from the scattered field $\boldsymbol{E}_{s,PO}$ (PO approach) with the RCS of its two components: the reflected one $\boldsymbol{E}_{s,PO+}$ and the FS one $\boldsymbol{E}_{s,PO-}$.

[38] Like for the first case, the reflected component decreases in the shadow region ($\boldsymbol{E}_{s,PO+}$ being negligible in Ω_4), and the FS component becomes the main contribution to the scattered field. Figure 17 compares the RCS of the FS component of PO with the RCS obtained by applying BP on the whole target.

[39] Here the two approaches do not match. Indeed, here $C_{Ba} \neq C_{PO}$: the contour of the surface Σ_{PO} (contour of the surface S_5) is different from that of the complementary Babinet screen Σ_{Ba} due to the equivalent rotation of the target. As already written, moving the transmitter with a fixed target is equivalent to rotating the target with a fixed transmitter. This case is equivalent to that of a normal incidence (like for the first case) but with a rotated pyramidal target with an angle

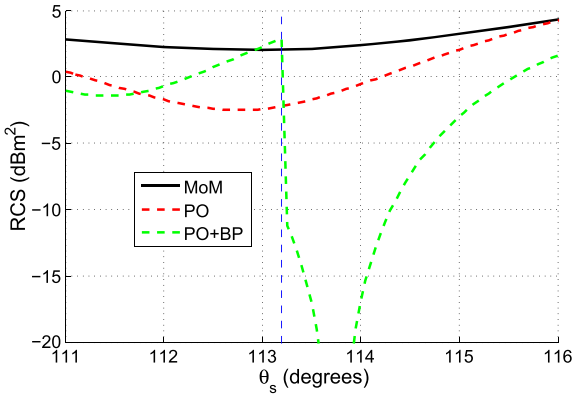

Figure 15. Enlarged detail of Figure 12 around the boundary between Ω_3 and Ω_4.

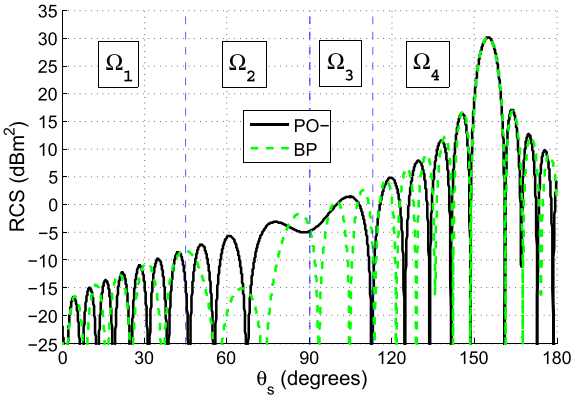

Figure 17. Same simulation parameters as in Figure 12 but computed from PO in forward scattering and BP.

of 25°. Thus, the proof detailed in section 2.3 is only satisfied when $\varphi(x,y) = 0$ implying $b_1 = b_2 = b_3 = 0$, which occurs for $\theta_s = \theta_i$ and $\phi_s = \phi_i$: this corresponds to the FS direction, for which $\boldsymbol{k}_i$ and $\boldsymbol{k}_s$ are collinear. Indeed, as can be seen in Figure 17, a perfect agreement is obtained in the FS direction $\theta_s = \theta_i = 155°$. The Babinet principle can be seen as an approximation of the PO approach which provides exactly the same results as the PO in the FS direction.

4. Conclusion

[40] For a three-dimensional (3-D) problem, this paper shows that the Babinet principle (BP) can be derived from the physical optics (PO) approximation. Indeed, following the same idea as Ufimtsev, from the PO approximation and in the far-field zone, the field scattered by an object can be split up into a field which mainly contributes around the specular direction (illuminated zone) and a field which mainly contributes around the forward direction (shadowed zone), which is strongly related to the scattered field obtained from the BP. The only difference resides in the integration surface.

[41] A theoretical study provided the mathematical proof that the involved integral in the FS component of PO does not depend on the global shape of the object. This corresponds to a demonstration of the shadow contour theorem which is different from that of Ufimtsev, since it considers here a PEC object of arbitrary shape, not two blackbodies (a PEC object being a more general case of the blackbody since the reflection is also considered). Moreover, the behavior of the reflected component of PO in the shadow zone is studied theoretically. Then, when the contour of Σ_{PO} is the same as the one of the complementary Babinet screen Σ_{Ba}, BP exactly corresponds to the FS component of PO. Thus, BP is contained in the PO approximation. When the two contours are not the same, BP can be seen as a good approximation of the PO approach, and BP provides exactly the same results as PO in the FS direction. These theoretical conclusions were illustrated with the scattering from a pyramidal target to better investigate the link between BP and PO.

References

Bakker, B. B., and E. T. Copson (1939), *The Mathematical Theory of Huygens Principle*, University Press, Oxford.

Booker, H. G. (1946), Slot aerials and their relation to complementary wire aerials (Babinet's principle), *Proc. IEE (London)*, *93*, 620–626.

Born, M., and E. Wolf (1959), *Principles of Optics*, Pergamon, New York.

Glaser, J. I. (1985), Bistatic RCS of complex objects near forward scatter, *IEEE Trans. on Aero. and Electron. Sys.*, *21*(1), 70–78.

Glaser, J. I. (1989), Some results in the bistatic radar cross section (RCS) of complex targets, *Proceedings of the IEEE*, *77*(5), 639–648.

Gordon, W. B. (1975), Far-field approximations to the Kirchhoff-Helmholtz representations of scattered fields, *IEEE Trans. Antennas Propag. Mag.*, *23*, 590–592.

Kildal, P. S., A. A. Kishk, and A. Tengs (1996), Reduction of forward scattering from cylindrical objects using hard surfaces, *IEEE Trans. Antennas Propag.*, *44*(11), 1509–1520.

Kubické, G., Y. A. Yahia, C. Bourlier, N. Pinel, and P. Pouliguen (2011), Bridging the gap between the Babinet principle and the physical optics approximation: Scalar problem, *IEEE Trans. Antennas Propag. Mag.*, *59*(12), 4725–4732.

Pouliguen, P., J. F. Damiens, and R. Moulinet (2003), Radar signatures of helicopter rotors in great biostatics, *Proc. APS/URSI'03, Columbus, USA*, *3*, 536–539.

Poincelot, P. (1957), Sur le théorème de Babinet au sens de la théorie électromagnétique, *Annales Télécommon.*, *12*, 410–413.

Siegel, K. M. (1958), Bistatic radars and forward scattering, *Aero Electronics Nat. Conf. Proc., Dayton, Ohio*, 286–290.

Ufimtsev, P. Y. (1990), Blackbodies and shadow radiation, *Sob. J. Commun. Technion. Electron. [translation from Russian by Scripta Technicsa, Inc.]*, *35*(5), 108–116.

Ufimtsev, P. Y. (1992), Blackbodies and the problem of invisible objects. *JINA'92*.

Ufimtsev, P. Y. (2007), *Fundamentals of the Physical Theory of Diffraction*, John Wiley, New Jersey.

Ufimtsev, P. Y. (2008), New insight into the classical MacDonald physical optics approximation, *IEEE Trans. Antennas Propag. Mag.*, *50*(3), 11–20.

Ufimtsev, P. Y. (2009), *Theory of Edge Diffraction in Electromagnetics—Origination and Validation of the Physical Theory of Diffraction*, Scotch Publishing Inc., Raleigh.